AN ABSTRACT OF THE THESIS OF

Ridwan Azam for the degree of Master of Science in Electrical and Computer Engineering presented on December 7, 2016.

Title: Comparison of Direct Drive Hydraulic and Dual-Stator Spoke Array Vernier Permanent Magnet Machines For Ocean Wave Energy Conversion

Abstract approved: ______________________________

Ted K.A. Brekken

Recently, there has been peaked interest in developing high energy producing and optimized power take-off topologies for Wave Energy Converters (WEC). As large as the potential of the oceans may seem, harnessing that energy and effectively converting it to electricity in significant amounts is a challenge. Currently, there are no single devices that satisfy this sufficiently. In this thesis we compare two promising Power Take-Off (PTO) units; the Dual-Stator Spoke Array Vernier Permanent Magnet machine (DSSA VPM) and the Direct Drive Hydraulic Power Take-Off (DDHPTO). A steady state and transient analysis is done to compare the efficiencies of the two machines. The results will show that the DSSA VPM has the higher efficiency and a greater Annual Energy Production (AEP) over the DDHPTO.

Comparison of Direct Drive Hydraulic and Dual-Stator Spoke Array Vernier Permanent Magnet Machines For Ocean Wave Energy Conversion

by

Ridwan Azam

A THESIS

submitted to

Oregon State University

in partial fulfillment of
the requirements for the
degree of

Master of Science

Presented December 7, 2016
Commencement June 2017

Master of Science thesis of Ridwan Azam presented on December 7, 2016.

APPROVED:

Major Professor, representing Electrical and Computer Engineering

---

Director of the School of Electrical Engineering and Computer Science

---

Dean of the Graduate School

I understand that my thesis will become part of the permanent collection of Oregon State University libraries. My signature below authorizes release of my thesis to any reader upon request.

Ridwan Azam, Author

ACKNOWLEDGEMENTS

I would like to begin expressing my sincere gratitude to my adviser Dr. Ted Brekken, for providing guidance, experience and knowledge, as well as his patience and enthusiasm to make this research a success. His routine meetings and hours of help made it possible for me to stay motivated and on track.

Secondly, I would like to express my heartfelt appreciation for Dr. Eduardo Cotilla-Sanchez, without whom I would not be in the Master program to begin with. It was due to him recruiting me on my senior year of undergrad that I was able to make it this far today.

Last but not least, I would like to thank all my friends, my fellow energy system group members, and my family. I was able to make it through due to their continued support and faith in me.

TABLE OF CONTENTS

LIST OF FIGURES

LIST OF TABLES

Chapter 1: Introduction

1.1 Motivation

Wave energy has an estimated untapped potential of around 8,000 to 80,000 TWh/y (1-10 TW), which is within the same order of magnitude as the world's electrical energy consumption [1]. This abundant resource is well worth any research exploits as it has a limited environmental impact, high energy density and it's free. The significant problem however, is harnessing that wave energy and converting it to electricity in large quantities. The waves are slow, random and have varying power levels. To design a device that can efficiently capture these irregular waves into smooth electrical power is quite the challenge. The device would also have to withstand extreme wave conditions that occur very rarely, but could have power levels in excess of 2000 kW/m [2]. Even though wave energy has among the highest energy density out of all renewable resources, wind and solar remain the leading powerhouses in clean energy production [3]. To date, only a few experimental wave generator plants are in operation around the world. The primary developers are located in USA, UK, Australia, Denmark, India, Ireland, Japan, Norway, Portugal, and The Netherlands [4].

As wave energy is still a developing field, model testing and improvements will keep on being conducted until a perfected model is produced. Our research builds upon a novel dual-stator spoke array vernier permanent magnet machine [5] and a direct drive hydraulic power take off architecture. The system requirements for the analysis have been determined through collaboration with Dehlsen Associates (DA). The results will show an analysis of steady state and transient efficiencies of both topologies. The transient sea state analysis will give the Annual Energy Production (AEP).

1.2 Literature Review

In this work we evaluate and compare the design of two power take-off topologies for point absorber wave energy converters. A point absorber is a device that possesses small dimensions relative to the incident wavelength. In this case, it is a floating structure that heaves up and down on the surface of the water. Due to their symmetry, wave direction is not an important factor for these devices [2]. The power take-off system grants the means to control the device and in doing so, it optimizes the energy transferred from the incident waves to the WEC [6].

Comparisons between electrical linear generators and hydraulic PTOs have been conducted in previous research [6, 7]. It was concluded from the results that the electrical system is more efficient than the hydraulic system, but, to generate the same power output, the electrical machine needs to be larger, leading to greater costs due to permanent magnets, which are made from rare earth materials. The hydraulic systems studied did have a smoother power output, but it required more maintenance and needed to be sealed correctly to remain watertight. [7]. However, due to the heavier build and higher cost of the electrical machine, Bard [6] concluded that the hydraulic system is a more reasonable choice for WEC commercialization, even though it requires further research on efficiency and reliability.

Chapter 2: Direct Drive Hydraulic Power Take-Off Model

2.1 DDHPTO Overview

Wave energy conversion is considered a suitable application for hydraulics. Waves apply large forces at slow speeds and hydraulic systems are suited to absorbing energy under this regime [8].

This hydraulic PTO is similar to a rack and pinion, in that it transfers the linear motion directly to rotational motion without rectifying or smoothing the flow. This results in a simple solution in terms of part count at the expense of more losses in mechanical to electrical conversion due to sub-optimal operating conditions for the electric generator.

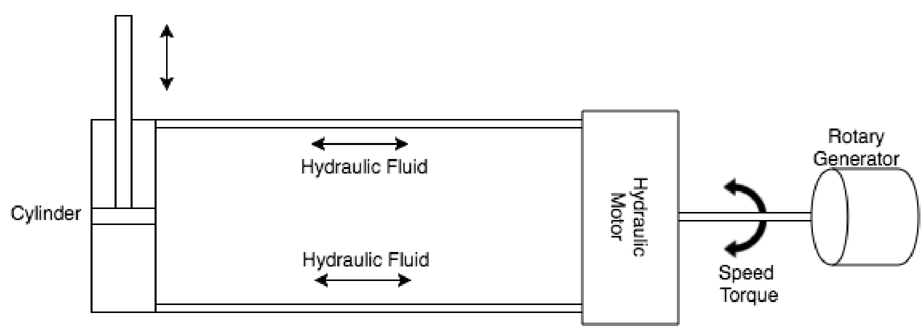

Figure 2.1: Direct drive hydraulic PTO

The direct drive hydraulic PTO shown in Fig. 2.1 consists of a cylinder, hydraulic motor and generator. The arrows depict the bi-directional course of flow.

2.2 Cylinder

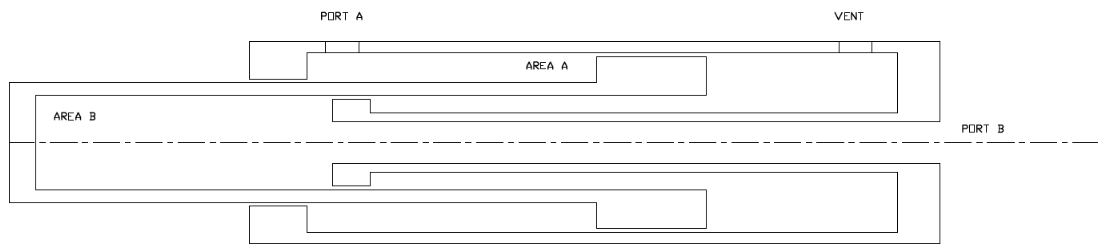

Figure 2.2: Folded actuator side cross section

The cylinder itself is a dual acting "folded actuator" as shown in Figure 2.2. This type of cylinder allows for operation in both directions to achieve an identical pressure given the same input force, whereas, traditional cylinders have the acting area of the piston reduced by the cylinder shaft on one side resulting in unequal pressures depending on the direction of applied force. Traditional cylinders also need to factor in the maximum load it can handle before it buckles. This is known as critical buckling load and can be defined in the Euler's Column Formula [9] :

$$F_{cr} = \frac{n \cdot \pi \cdot 2 \cdot E \cdot I}{L^2} \tag{2.1}$$

Where F_{cr} is the critical load value, n is the factor accounting for the end conditions (fixings), E is the modulus of elasticity [9], I is the moment of inertia, and L is the unsupported length of the rod. With this equal pressure cylinder design we can customize the rod diameter and internal bore of the rod as well. These controllable design parameters prevent buckling to be a design driver with respect to the pressure and flow.

2.3 Hydraulic Motor

The hydraulic motors used in this system are manufactured by Bosch Rexroth [10]. The hydraulic motor system is comprised of two axial piston fixed displacement motors connected together via a common drive shaft to accommodate for incoming force and velocity, as there are no motors made to date that can handle the system requirements alone. In that regard, a 750 cm^3/rev and a 1000 cm^3/rev motor is chosen for the combined hydraulic motor system, which will then be connected to a generator.

2.4 Generator

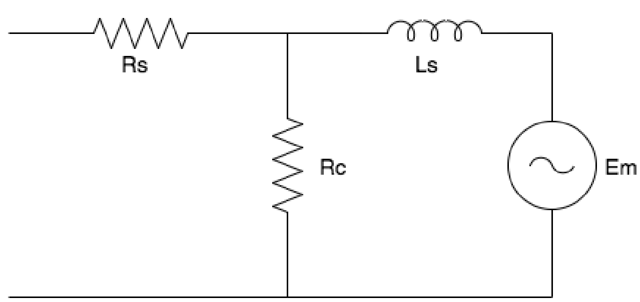

Figure 2.3: Equivalent electric circuit model of generator

The generator is a traditional permanent magnet synchronous generator with a rated speed of 1800 rpm. An equivalent circuit of the generator is shown in Figure 2.3. The per phase circuit consists of a series resistor R_s at the input terminals, representing the I^2R loss in the stator windings, a shunt resistor R_c representing the core loss, a stator inductance L_s and a back-emf voltage E_m.

2.5 DDHPTO Formulation and Simulink Model

The electric power output is calculated as follows:

$$\omega_m = \frac{Q}{D_T} \tag{2.2}$$

$$Q = V \cdot A_p \tag{2.3}$$

$$T_m = P \cdot D_T \cdot \eta_m \tag{2.4}$$

$$P = \frac{F_{PTO}}{A_p} \tag{2.5}$$

$$T_{gen} = T_m - \omega_m \cdot \frac{dJ_T}{dt} \tag{2.6}$$

where ω_m is the motor speed, Q is the volumetric flow, D_T is the combined motor displacement, V is the PTO heave velocity, A_p is the piston area of the cylinder,

T_m is the motor torque, P is the pressure applied across the motor ports, η_m is the combined motor efficiency, T_{gen} is the generator torque, and J_T is the combined motor and generator torque. The electric power is then selected by a look-up table based on individual torque and speed values and the operating generator efficiency at each intersecting point. The Simulink model is shown in Figure 2.4.

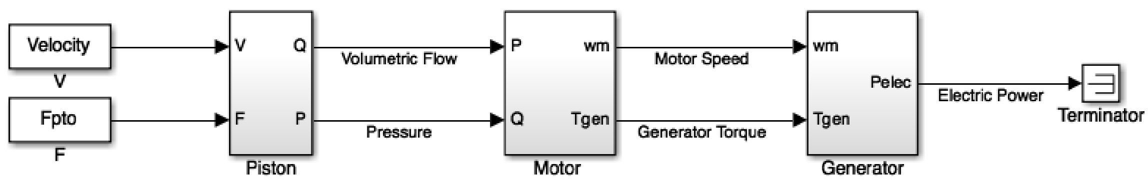

Figure 2.4: Simulink model of the DDHPTO

Chapter 3: Vernier Permanent Magnet Linear Generator

3.1 VPMLG Overview

Vernier Permanent Magnet (VPM) machines represent a special class of permanent magnet synchronous electrical machine. The VPM utilize higher order space harmonics of the air gap magnetic field due to the multiphase stator winding currents that are contained in open slots at the air gap surface of the stator structure. Conventional PM synchronous machines employ only the fundamental component of the air gap magnetic field due to the slotted stator winding currents. A major disadvantage of the VPM machine is its low power factor [11, 12]. Therefore, a Dual-Stator Spoke Array Vernier Permanent Magnet (DSSA VPM) machine was introduced to eradicate that disadvantage. Finite Element Analysis (FEA) and prototype experimentation proved that the DSSA VPM machine induces a higher torque density than regular VPM machines and comparable power factor with the traditional permanent magnet machines [5].This machine is suitable for direct drive applications, based on its magnetic gearing. Small movements of the translator create large changes in flux resulting in high steady torque generation, which is known as the gearing effect [13].

3.2 VPMLG Design

The direct drive generator with translator is shown in the high-level model Figure 3.1. The vertical arrow indicates direction of oscillation. This structure is a single floating device, tethered to the ocean floor, with a transmission line connected to a storage device or the grid.

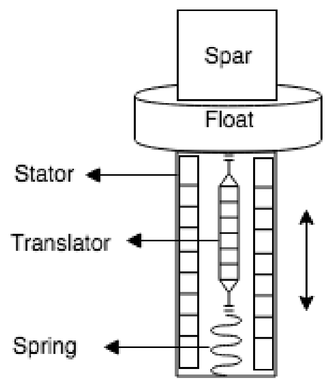

Figure 3.1: Direct drive vernier permanent magnet linear generator

3.3 VPMLG Formulation and Simulink Model

The voltage, currents, and electrical power in the d-q reference frame are formulated as follows:

$$v_d = R_d \cdot i_d + \frac{d\lambda_d}{dt} - \omega_d \cdot \lambda_q \tag{3.1}$$

$$v_q = R_q \cdot i_q + \frac{d\lambda_q}{dt} + \omega_d \cdot \lambda_d \tag{3.2}$$

$$i_d = 0 \tag{3.3}$$

$$i_q = \frac{F_{PTO} \cdot \tau_p}{\lambda_{fd} \cdot \pi} \tag{3.4}$$

$$\lambda_d = L_d \cdot i_d + \lambda_{fd} \tag{3.5}$$

$$\lambda_q = L_q \cdot i_d \tag{3.6}$$

$$P_{dq\_coreloss} = \frac{v_d^2}{R_c} + \frac{v_q^2}{R_c} \tag{3.7}$$

$$P_{elec} = v_d \cdot i_d + v_q \cdot i_q + P_{dq\_coreloss} \tag{3.8}$$

where v$_d, v_q, i_d, i_q$,λ_d, λq, L_d, and L_q are the d-q voltages, currents, flux linkages and inductances, respectively R_d, R_q, and R_c are the d-q series resistance at the input terminals and shunt resistor representing core loss, ω_d is the synchronous speed, F_{PTO} is the input PTO force, τ_p is the translator pole pitch, λ_{fd} is the d-axis flux linkage, $P_{dq\_coreloss}$ is the d-q core losses, and P_{elec} is the electrical power output for one side of the machine. The the d-axis is aligned with the translator; therefore, the current, i_d, is zero for (3.3), assuming no flux weakening.

The Matlab Simulink model of the direct drive VPMLG is shown in Figure 3.2. The model shows one side of the machine; however, since both stators are identical and are drive balanced and phase locked to each other, simply multiplying the output by a factor of 2 will give the power output of the whole machine.

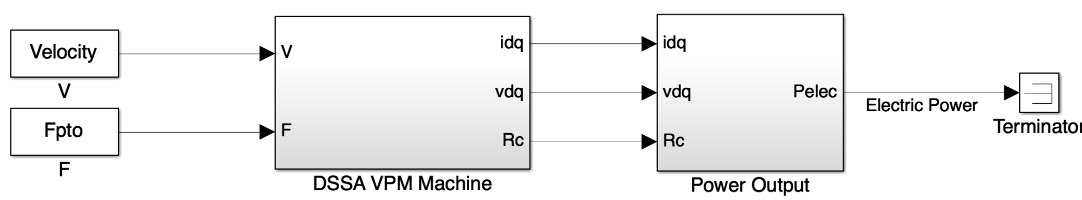

Figure 3.2: Simulink model of direct drive vernier permanent magnet linear generator

Chapter 4: Simulations Results and Analysis

To assess the impact of maximum Power Take Off (PTO) force on Annual Energy Production (AEP), Dehlsen Associates (DA) computed a power matrix for the Centipod [14] using Model Predictive Control (MPC) [15] with 200 kN, 400 kN, 600 kN, and 1000 kN as F_{PTO} max limit within the controller. These power matrices were computed per the Department of Energy (DOE) Levelized Cost Of Energy (LCOE) guidance specification of $200 \cdot T_e$ time series Bretschneider spectrum for each of the 114 sea state bins in the Northern California reference resource Joint Probability Matrix (JPD) [16].

4.1 System Requirements

The system requirements for the topologies are outlined in Table 4.1.

Table 4.1: PTO System Requirements

	Value	Unit
Max F_{PTO}	600	kN
Max dF_{PTO}	1000	kN/s
Max Velocity	1.5	m/s
Stroke	4	m

The main control parameters for development and the design of the two machines were the maximum F_{PTO} and the maximum wave speed. DA set the maximum force to 600 kN based on its impact on minimizing the LCOE. The maximum PTO velocity was explored using the time series output of the 114 sea state simulations, and a maximum speed of 1.5 m/s was set, as the majority of the energy extraction occurred below that. The range of forces and velocities provided by DA are shown on the graphs below, including the power waves based for each machine.

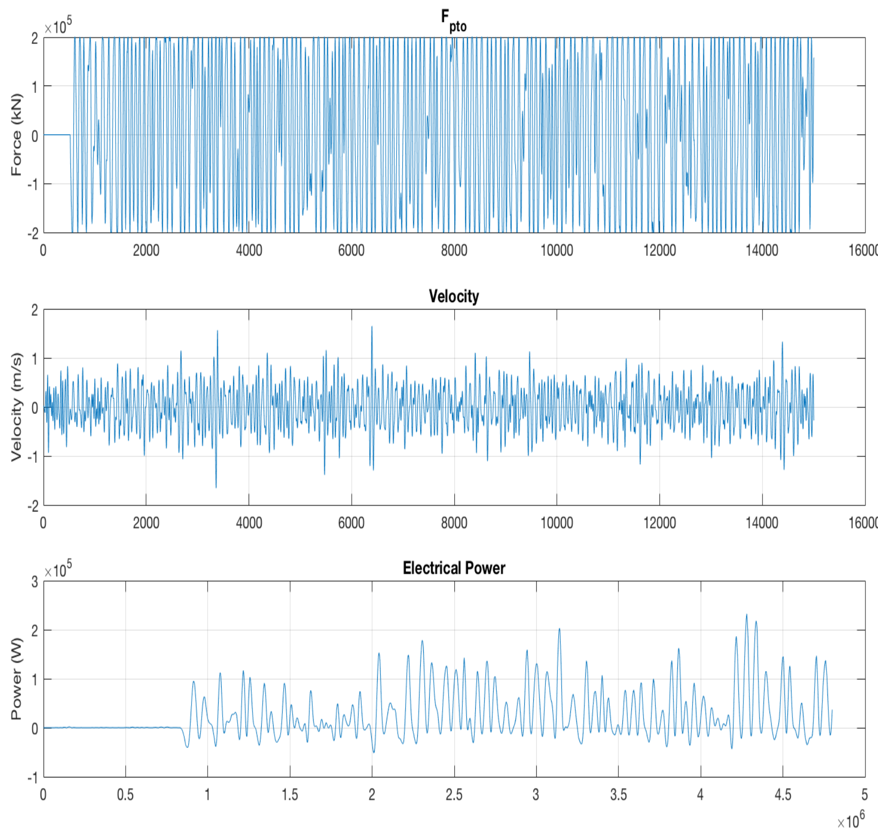

Figure 4.1: F_{PTO}, Velocity and Power for VPMLG

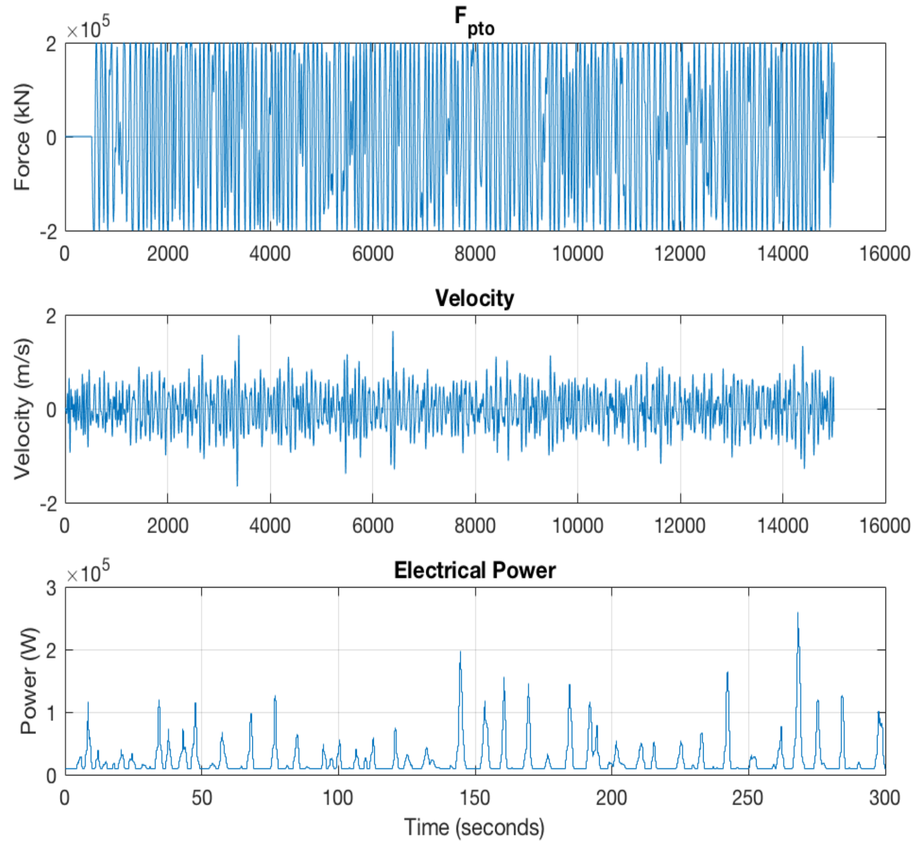

Figure 4.2: F_{PTO}, Velocity and Power for DDHPTO

The following graphs match the JPD for the northern California wave resource (the DOE uses this as a standard for cost of energy calculations). The JPD gives the percentage chance of a certain sea state occurring on an annual basis. The efficiency in the transient results are applied directly on a sea state by sea state basis and multiplied by the probability of that sea state occurring. The JPD comes from real measured buoy data; the results are lumped into discrete bins. For example, for sea states that produce vertical PTO heave velocities (dz) between

1.0 and 1.10 m/s, that bin is labeled 1.05 m/s since it is the center of the range that bin represents. All the bins are then summed up to get AEP.

4.2 Steady State

Steady state efficiency matrices were created for each of the PTO topologies investigated using the machine parameters calculated. These matrices cover all operating points between zero and the defined constraint for force and velocity (600 kN, and 1.5 m/s respectively) with bin widths of 50 kN and 0.1 ms.

Comparing the steady state efficiency matrices for both the topologies, it is shown that for any operating point in the sea state, the VPMLG in Figure 4.3 has a higher efficiency than the DDHPTO Figure 4.4. For example, in one case, where the operating efficiency at 125 kN and 1.45 m/s, is 53.5% in the DDHPTO, it is 93.2% for the VPMLG. Thus, proving that for the steady state analysis the VPMLG is by far the more efficient machine.

PTO Efficiency by Operating State

dz(m/s) - center of bin \ Fpto(kN) - center of bin	25	75	125	175	225	275	325	375	425	475	525	575
1.45	0.671	0.889	0.932	0.949	0.958	0.964	0.967	0.969	0.971	0.972	0.972	0.972
1.35	0.674	0.890	0.932	0.949	0.958	0.964	0.967	0.969	0.970	0.971	0.971	0.971
1.25	0.677	0.891	0.932	0.949	0.958	0.963	0.967	0.968	0.970	0.970	0.970	0.970
1.15	0.679	0.891	0.933	0.949	0.958	0.963	0.966	0.968	0.969	0.969	0.969	0.969
1.05	0.682	0.892	0.933	0.949	0.958	0.963	0.965	0.967	0.968	0.968	0.968	0.968
0.95	0.685	0.893	0.933	0.949	0.957	0.962	0.964	0.966	0.966	0.967	0.966	0.966
0.85	0.688	0.894	0.933	0.949	0.957	0.961	0.963	0.964	0.965	0.965	0.964	0.963
0.75	0.690	0.894	0.933	0.948	0.956	0.960	0.962	0.963	0.963	0.962	0.962	0.961
0.65	0.693	0.895	0.933	0.948	0.955	0.958	0.960	0.960	0.960	0.959	0.958	0.957
0.55	0.696	0.895	0.932	0.947	0.953	0.956	0.957	0.957	0.956	0.955	0.953	0.951
0.45	0.698	0.895	0.931	0.945	0.950	0.953	0.953	0.952	0.951	0.949	0.946	0.944
0.35	0.701	0.895	0.929	0.942	0.946	0.947	0.946	0.944	0.942	0.938	0.935	0.931
0.25	0.703	0.893	0.926	0.936	0.938	0.937	0.934	0.930	0.925	0.920	0.915	0.909
0.15	0.705	0.888	0.916	0.921	0.919	0.913	0.905	0.897	0.887	0.878	0.867	0.857
0.05	0.702	0.861	0.865	0.847	0.821	0.792	0.761	0.729	0.697	0.664	0.630	0.597

Figure 4.3: Steady State efficiency of VPMLG

PTO Efficiency by Operating State

dz(m/s) - center of bin \ Fpto(kN) - center of bin	25	75	125	175	225	275	325	375	425	475	525	575
1.45	0.259	0.454	0.535	0.595	0.646	0.689	0.726	0.758	0.784	0.805	0.821	0.832
1.35	0.308	0.503	0.580	0.636	0.683	0.722	0.756	0.784	0.807	0.826	0.839	0.849
1.25	0.356	0.549	0.622	0.674	0.716	0.751	0.781	0.806	0.827	0.843	0.855	0.862
1.15	0.403	0.591	0.659	0.707	0.745	0.777	0.803	0.825	0.843	0.857	0.867	0.873
1.05	0.448	0.630	0.693	0.736	0.770	0.798	0.822	0.841	0.856	0.868	0.876	0.880
0.95	0.489	0.663	0.722	0.761	0.791	0.816	0.836	0.853	0.866	0.875	0.881	0.884
0.85	0.528	0.693	0.746	0.781	0.808	0.829	0.847	0.861	0.871	0.879	0.883	0.885
0.75	0.563	0.718	0.766	0.797	0.820	0.839	0.853	0.865	0.873	0.879	0.882	0.882
0.65	0.595	0.738	0.781	0.808	0.828	0.844	0.856	0.865	0.871	0.875	0.876	0.875
0.55	0.622	0.753	0.792	0.815	0.831	0.844	0.854	0.860	0.865	0.867	0.866	0.864
0.45	0.644	0.763	0.797	0.816	0.830	0.839	0.846	0.851	0.853	0.853	0.851	0.847
0.35	0.661	0.768	0.796	0.812	0.822	0.828	0.832	0.834	0.834	0.831	0.828	0.822
0.25	0.672	0.766	0.788	0.799	0.805	0.808	0.808	0.806	0.803	0.798	0.791	0.783
0.15	0.677	0.755	0.769	0.773	0.772	0.768	0.762	0.754	0.744	0.733	0.720	0.706
0.05	0.668	0.712	0.698	0.673	0.645	0.613	0.580	0.544	0.507	0.469	0.430	0.390

Figure 4.4: Steady State Efficiency of DDHPTO

4.3 Transient

Machine performance was further explored through the creation of a Simulink model which could simulate the transient performance of the machine. This exercise is more intensive than the steady state analysis and therefore, it was used to check the suitability of the completed analysis on each of the PTO topologies.

H_{m0} is significant wave height in meters. This is roughly equal to the mean of the largest third of the individual wave heights in the time series sample.

T_e is the energy period in seconds. Energy period is the period that a given time series would have if every wave were a fixed period to produce the same power [17], which is defined as:

$$\text{Power} = 0.49 \cdot H_{m0}^2 \cdot T_e \tag{4.1}$$

The previous performance analysis used in this study applied an efficiency matrix of steady state force and velocity combinations to a probability of those conditions occurring to produce a close but optimistic approximation of AEP for the topologies. The Simulink model of the VPMLG machine in Figure 4.5 showed an AEP only 1% below the original predicted value.

The same process was carried out for the DDHPTO topology in Figure 4.6. The Simulink model of the linear to rotary hydraulic machine showed an AEP only 2% below the original predicted value.

The transient analysis showed an AEP only a couple percent below what had been predicted via the steady state efficiency method for both machines, proving that for the purposes of this study the steady state performance assessment alone would have been sufficient to compare the efficiencies.

Efficiency of PTO		Te (s), center of bin																				
		0.5	1.5	2.5	3.5	4.5	5.5	6.5	7.5	8.5	9.5	10.5	11.5	12.5	13.5	14.5	15.5	16.5	17.5	18.5	19.5	20.5
Hm0 (m), center of bin	0.25								0.54	0.59												
	0.75					0.94	0.92	0.91	0.90	0.88	0.85	0.85	0.79	0.74								
	1.25					0.96	0.94	0.94	0.92	0.89	0.88	0.85	0.87	0.84	0.85	0.83	0.84					
	1.75						0.95	0.94	0.90	0.90	0.89	0.91	0.89	0.89	0.89	0.88	0.88					
	2.25							0.93	0.92	0.92	0.92	0.92	0.92	0.90	0.91	0.90	0.91	0.90				
	2.75							0.95	0.94	0.94	0.94	0.94	0.93	0.92	0.92	0.92	0.92	0.91				
	3.25								0.94	0.94	0.94	0.94	0.94	0.94	0.93	0.93	0.93	0.92	0.92	0.91		
	3.75								0.95	0.95	0.95	0.95	0.94	0.95	0.94	0.94	0.93	0.93				
	4.25									0.95	0.95	0.95	0.95	0.95	0.95	0.95	0.94	0.93				
	4.75									0.96	0.96	0.95	0.95	0.95	0.95	0.95	0.93	0.93				
	5.25										0.95	0.95	0.95	0.95	0.95	0.95	0.94					
	5.75												0.95	0.95	0.95	0.93	0.92					
	6.25													0.95	0.95	0.91	0.91					
	6.75														0.94	0.93						
	7.25																					
	7.75																					
	8.25																					
	8.75																					
	9.25																					
	9.75																					

Figure 4.5: Transient state efficiency of VPMLG

Efficiency of PTO		Te (s), center of bin																				
		0.5	1.5	2.5	3.5	4.5	5.5	6.5	7.5	8.5	9.5	10.5	11.5	12.5	13.5	14.5	15.5	16.5	17.5	18.5	19.5	20.5
Hm0 (m), center of bin	0.25								0.74	0.77												
	0.75					0.41	0.64	0.73	0.78	0.82	0.85	0.86	0.86	0.84								
	1.25					0.4	0.6	0.72	0.79	0.84	0.85	0.87	0.86	0.85	0.84	0.84	0.84					
	1.75						0.6	0.71	0.81	0.84	0.85	0.86	0.86	0.86	0.85	0.85	0.84					
	2.25							0.71	0.78	0.82	0.84	0.85	0.85	0.85	0.85	0.84	0.84	0.84				
	2.75							0.67	0.76	0.79	0.81	0.83	0.84	0.85	0.85	0.85	0.85	0.84				
	3.25								0.73	0.77	0.8	0.81	0.83	0.84	0.84	0.84	0.84	0.84	0.83	0.83		
	3.75								0.69	0.74	0.77	0.8	0.82	0.83	0.83	0.84	0.84	0.83				
	4.25									0.71	0.76	0.78	0.8	0.81	0.83	0.83	0.83	0.83				
	4.75									0.67	0.72	0.76	0.78	0.81	0.82	0.82	0.81	0.82				
	5.25										0.7	0.75	0.77	0.79	0.81	0.81	0.82					
	5.75												0.76	0.78	0.79	0.8	0.8					
	6.25													0.76	0.78	0.74	0.78					
	6.75														0.76	0.78						
	7.25																					
	7.75																					
	8.25																					
	8.75																					
	9.25																					
	9.75																					

Figure 4.6: Transient state efficiency of DDHPTO

Chapter 5: Conclusion and Future Work

5.1 Summary and Conclusions

he considerable potential of wave energy is a significant lure to generating electricity. Research and development will keep on going into this vast resource until efficient and marketable models are made. There are still design challenges that prove difficult to solve. Although, simulation results may prove more than promising, the manufacturing and live testing will always have factors that are unaccounted for. Beyond producing a single device, individual WECs will need to operate in tandem to provide sufficient power in farms, therefore, analysis will need to be conducted to optimize that.

This research provided a comparison between two wave energy conversion topologies, a novel Dual-Stator Spoke Array Vernier Permanent Magnet (DSSA VPM) machine and a Direct Drive Hydraulic Power Take-Off (DDHPTO) model. It was stated from previous research that while the electrical linear generators were more efficient, they were heavier and more costly than the the hydraulic machines and that the hydraulic machines were more reasonable for commercialization. These results show that the efficiencies of the VPMLG is much higher than the DDHPTO to make it a reasonable choice for commercialization. The machines were tested by a steady state and transient efficiency analysis. The final results showed that while the transient to steady state AEP ratios were about 1% off for each, the AEP of the VPMLG machine was 16% higher than the DDHPTO. Future work will implement model predictive control to the VPMLG machine for optimal wave energy conversion within system limits. Model predictive control will be done via reactive control which will be discussed further in the section below.

5.2 Future Work

Wave energy is captured most efficiently when the frequency of a realistic irregular sea state is close to that of the resonant frequency of the wave converter [18]. During resonance, the velocity of the oscillator is in phase with the dynamic force of an incoming wave, resulting in a significant transfer of energy from the wave to the oscillator [19].

It is shown by Falnes, that the maximum energy converted at any frequency w is obtained under the following condition:

$$F_u(w) = -Z_i^*(w) \cdot u(w) \tag{5.1}$$

$$Z_i(w) = R_i(w) - X_i(w) \tag{5.2}$$

where $F_u(w)$ is the optimal load force, Z_i is termed the intrinsic mechanical impedance which is the mechanical impedance of the oscillating system, respectively $R_i(w)$ and $-X_i(w)$ are the real and imaginary part of the impedance and $u(w)$ is the oscillating speed.

The condition can be met through reactive control, alternatively termed complex-conjugate control. It is known as reactive control, due to the fact that the imaginary part of Z_i^* cancels the imaginary part of Z_i. Complex-conjugate control refers to the fact that the optimal load impedance has to match the complex-conjugate of the intrinsic impedance Z_i^* [20]. This is analogous to electrical AC power systems, hence the names.

$$S = I^* \cdot V \tag{5.3}$$

$$S = P + iQ \tag{5.4}$$

The complex power, S is the product of the conjugate of current, I and the voltage, V. The complex power can also be split into it's real, P and imaginary, Q parts. Based on the P and Q values, S will determine whether it is absorbing or delivering power. In generator convention, where current is leaving the positive terminal of the circuit element, if Q is positive then the reactive power is delivered back into the system [21].

In order to achieve optimum condition, reactive power is needed for the WEC. This means that rather than just absorbing power, the device will deliver some energy back to the ocean during part of the oscillation cycle. The reason for doing so, is to improve the phase alignment between the oscillating velocity and the dynamic force of the incoming wave, which will lead to resonant operation.

Bibliography

[1] http://www.renewableuk.com/.

[2] B. Drew, A. Plummer, and M. Sahinkaya., “A Review of Wave Energy Converter Technology,” in *Part A: Journal of Power and Energy*, pp. 887902,Proceedings of the Institution of Mechanical Engineers, 2009.

[3] A. Clément, P. McCullen, A. Falcão, A. Fiorentino, F. Gardner, K. Hammarlund, G. Lemonis, T. Lewis, K. Nielsen, S. Petroncini, M.-T. Pontes, P. Schild, B.-O. Sjöström, H. C. Srensen, and T. Thorpe, “Wave Energy in Europe: Current Status and Perspectives,” *Renewable and Sustainable EnergyReviews*, vol. 6, no. 5, pp. 405431, 2002.

[4] H. Bernhoff and M. Leijon,“Conversion of Wave Energy to Electricity,” Nov 2006.

[5] D. Li, R. Qu, W. Xu, J. Li, and T. A. Lipo, “Design Procedure of Dual-Stator Spoke-Array Vernier Permanent-Magnet Machines,” *IEEE Transactionson Industry Applications*, 2015.

[6] J. Bard and P. Kracht, “Report on Linear Generator Systems for Wave Energy Converters,” tech. rep., AALBORG University, 2013.

[7] C. Boström, “Electrical systems for wave energy conversion,” 2011.

[8] R. Henderson, "Design, simulation, and testing of a novel hydraulic powertake-off system for the pelamis wave energy converter," *Renewable Energy*, vol. 31, no. 2, pp. 271–283, 2006.

[9] http://www.engineeringtoolbox.com/euler-column-formula-d1813.html.

[10] https://www.boschrexroth.com/ics/cat/?language=enid=cat=mobile-hydraulics-catalogm=xcu=sio=desktopp=g261597.

[11] E. Spooner and L. Haydock, "Vernier Hybrid Machines," *IEE Proceedings - ElectricPower Applications*, vol. 150, pp. 655–662, Nov 2003.

[12] D. Li, R. Qu, and Z. Zhu, "Comparison of Halbach and Dual-Side Vernier Permanentmagnet Machines," *IEEE Transactions on Magnetics*, vol. 50, pp. 801–804, Feb 2014.

[13] A. Toba and T. A. Lipo, Novel Dual-Excitation Permanent Magnet Vernier Machine, in *Conference Record of the 1999 IEEE Industry Applications Conference.Thirty-Forth IAS Annual Meeting (Cat. No.99CH36370)*, vol. 4, pp. 2539–2544, 1999.

[14] http://www.ecomerittech.com/centipod.php.

[15] https://mhkdr.openei.org/submissions/74.

[16] A. McCall, "Advanced Controls for the Multipod Centipod WEC Device," tech. rep.,Dehlsen Associates, 2016.

[17] J. B. Herbich, *Handbook of Coastal Engineering*. McGraw-Hill Professional, 1 ed., 2000.

[18] U. Korde, "Efficient Primary Energy Conversion in Irregular Waves," *Ocean Engineering*, vol. 26, no. 7, pp. 625–651, 1999.

[19] K. Budar and J. Falnes, "A Resonant Point Absorber of Ocean-Wave Power," *Nature*, vol. 256, p. 478, Aug 1975

[20] J. Falnes, *Ocean Waves and Oscillating Systems*. Cambridge University Press, 2002

[21] J. D. Glover, M. S. Sharma, and T. J. Overbye, *Power System Analysis and Design*. Global Engineering, 2012.